

Pulsed Ultrasonic Studies of the Acoustoelectric Effect, Ultrasonic Attenuation, and Trapping in CdS†

VICTOR E. HENRICH* AND GABRIEL WEINREICH

Department of Physics, University of Michigan, Ann Arbor, Michigan 48103

(Received 20 August 1968)

Ultrasonic attenuation and electron trapping in cadmium sulfide have been studied by means of the acoustoelectric effect. Pulses of 30-MHz ultrasound, short compared to the sample length, generate acoustoelectric current signals with a portion corresponding to the sound pulse entirely inside the sample. This portion should decay exponentially with a time constant proportional to the total ultrasonic attenuation, independent of bond losses, transducer efficiencies, etc. By varying the conductivity, the electronic and lattice parts of the attenuation can be separated. Available CdS crystals have rather inhomogeneous spatial impurity distributions which appear as spatial variations in the electron density. These variations distort the exponential decay of the acoustoelectric current, forcing us to formulate a model for the nonuniformity in order to explain the observed waveforms. This model gave good quantitative agreement with the data on one sample. The ultrasonic attenuation due to electrons was found to be accurately described by the theory of Hutson and White, and lattice attenuations of about 2 dB/cm were measured. Information on trapping parameters can be obtained from the magnitude of the acoustoelectric current. One sample showed strong evidence of trapping which could be explained by the presence of a trap 0.4 eV below the conduction band with a density of about $4 \times 10^{15} \text{ cm}^{-3}$.

INTRODUCTION

THE bulk of the acoustic work done on CdS has centered on the amplification, oscillation, and current saturation that exist when an external electric field is applied. Unfortunately, the behavior of CdS under conditions of gain is rather complicated.¹ Some problems are inherent in the processes themselves,² while others are due to the poor quality of presently available crystals. Because alternative interpretations are sometimes possible, the results of such experiments may be open to question.

In this paper we report a study of ultrasonic attenuation, electron trapping, and crystal impurity distribution by means of the acoustoelectric effect in the absence of any external electric field. Since the problems of noise and acoustic saturation that plague amplification experiments are entirely absent, and other complications enter to a much smaller degree, the interpretation of results in more straightforward and unequivocal.

In Sec. 1 we shall review briefly the relevant theory. The advantages of pulsed ultrasonic measurements will be discussed, and the computational extensions necessary to make full use of the method will be presented. In Sec. 2 the experimental methods will be outlined. In Sec. 3 a sample will be examined that behaves roughly as we would predict, although showing signs of spatial conductivity inhomogeneity. Section 4 will treat the first-order effects of such inhomogeneity on acoustoelectric measurements, and in Sec. 5 we shall examine in detail a sample which is readily amenable to this analysis and yields detailed information about ultrasonic attenuation and trapping.

† Work supported in part by the U. S. Atomic Energy Commission under Contract No. AT(11-1)-1112.

* Present address: Lincoln Laboratory, Massachusetts Institute of Technology, Lexington, Massachusetts 02173.

¹ J. H. McFee, Bell Laboratories Technical Memorandum 64-1352-22, 1964 (unpublished).

² D. L. White, *J. Appl. Phys.* **33**, 2547 (1962).

1. BASIC THEORY

Using a general argument based on conservation of energy and momentum between traveling ultrasonic waves and conduction electrons, Weinreich³ showed that the local electric field produced by a sound wave⁴ was given by

$$E_{AE} = \alpha_E W / q n_0, \quad (1)$$

where E_{AE} is the acoustoelectric field, α_E that part of the ultrasonic attenuation due to conduction electrons,⁵ q the electronic charge, n_0 the conduction electron density, and W the energy density of the ultrasonic wave.

Relation (1) can be expressed in terms of a current density by multiplying by the sample's conductivity:

$$J_{AE} = \sigma_0 E_{AE} = \mu \alpha_E W. \quad (2)$$

Here μ is the electron mobility.

The above relation holds regardless of the nature of the electron-phonon coupling. It does, however, assume that all the momentum absorbed by the electrons is removed by the acoustoelectric field, and therefore has to be modified in the presence of trapping.

Acoustodynamic effects in semiconductors, including the possibility of gain resulting from the application of an external electric field, were first analyzed by Weinreich.⁶ This analysis was extended by Hutson and White^{2,7} to the case of piezoelectric semiconductors such as cadmium sulfide. The latter authors made a number of important generalizations, such as the in-

³ G. Weinreich, *Phys. Rev.* **107**, 317 (1957).

⁴ The correct term for 30-MHz acoustic waves, used in our work, is "ultrasound", but for brevity we shall use "sound."

⁵ We consider only electron conduction since hole conduction is negligible or absent under all but a few special cases. See F. Chernow, E. Courtens, M. Douma, and L. Goodman, *Appl. Phys. Letters* **9**, 145 (1966).

⁶ G. Weinreich, *Phys. Rev.* **104**, 321 (1956).

⁷ A. R. Hutson and D. L. White, *J. Appl. Phys.* **33**, 40 (1962).

clusion of the effect of trapping mentioned above. Imposing the restriction that

$$\text{strain} \ll \epsilon v_s / f \mu e, \quad (3)$$

where v_s is the velocity of sound, e the piezoelectric

constant, f the fraction of acoustically produced space charge that is in the conduction band (i.e., not trapped), and ϵ the dielectric constant, they obtained the following expression for the ultrasonic attenuation due to electrons:

$$\alpha_E = \frac{1}{2} K^2 \frac{\sigma}{\epsilon v_s} \left(\frac{1 - (\omega/\omega_D) \text{Im}(f)}{[1 - (\omega/\omega_D) \text{Im}(f)]^2 + [\sigma/\epsilon\omega + (\omega/\omega_D) \text{Re}(f)]^2} \right). \quad (4)$$

Here ω is the acoustic frequency, ω_D the diffusion frequency defined by $\omega_D = v_s^2/D_n$, where D_n is the electron diffusion constant, and K^2 is the electromechanical coupling constant, defined in terms of the above quantities and the elastic constant c by $K^2 = e^2/\epsilon c$. It should be noted that because of finite trapping times, the fraction f is, in general, complex.

The Hutson-White theory gives expressions for such first-order quantities as the acoustically produced space charge (n_s) and the ac electric field accompanying the sound wave (E_1), in terms of which the acoustoelectric current can be calculated from

$$J_{AE} = \mu q \frac{1}{2} \text{Re}(E_1^* f n_s). \quad (5)$$

Putting the expressions in Eq. (2) in for E_1 and n_s , we get

$$J_{AE} = \mu \alpha_E W \text{Re}(f). \quad (6)$$

This is relation (2) modified to include trapping effects. In terms of E_{AE} it becomes

$$E_{AE} = \alpha_E W \text{Re}(f) / q n_0. \quad (7)$$

Equations (2) and (6) are point relations, and in order to express them in terms of parameters measured in an external circuit they must be integrated over the entire crystal. For sound traveling in the x direction, we have for the observed open-circuit acoustoelectric voltage

$$V_{AE} = \int_{\text{crystal}} E_{AE} dx. \quad (8)$$

If the crystal were short-circuited, the measured current would be

$$I_{AE} = V_{AE} / R_c, \quad (9)$$

where R_c is the crystal resistance.

In this experiment a pulsed ultrasonic field was used, with the pulse length always shorter than one acoustic transit time through the crystal. If we only consider times when the sound is entirely inside the crystal, and further assume that n_0 , f , α_E , and α_L (the component of ultrasonic attenuation due to the lattice) are constant throughout the crystal, we obtain

$$\begin{aligned} V_{AE}(t) &= \frac{\alpha_E \text{Re}(f)}{q n_0} \int_{\text{pulse}} W dx \\ &= \frac{\alpha_E \text{Re}(f) e^{-(\alpha_E + \alpha_L) v_s t}}{q n_0} \int_{\text{pulse}} W_0(x) dx, \end{aligned} \quad (10)$$

where $W_0(x)$ is the acoustic energy density at $t=0$. The last integral is independent of time, so that as long as the pulse is inside the crystal the observed voltage should decrease exponentially with time, with time constant

$$\tau = [(\alpha_E + \alpha_L) v_s]^{-1}. \quad (11)$$

It is the main purpose of this experiment to analyze the acoustoelectric waveforms from the standpoint of Eq. (11), since the exponential section of the waveforms provides an *absolute* measurement of the total attenuation in the crystal, independent of bond losses, transducer efficiencies, reflection and transmission coefficients, etc. By varying the illumination of the crystal, it is possible to separate α_E from α_L , since only α_E is a function of conductivity.

We will be interested here only in the small-signal regime, where the acoustoelectric voltage is merely proportional to acoustic power. The two interesting independent variables in this range are acoustic frequency and sample conductivity. All work reported here was done at constant frequency, using conductivity as the variable. Conductivity is particularly powerful as several orders of magnitude are available on each crystal merely by varying the illumination.

A. Trapping

The presence of $\text{Re}(f)$ in Eqs. (6) and (10) shows that it should be possible to get some information on electron trapping from acoustoelectric measurements. The effects of trapping have been studied by several authors,⁸⁻¹⁴ among them Greebe,⁸ who studied variations in acoustoelectric current as a function of acoustic frequency. He considers an extension of the method of Shockley and Read,¹⁵ which treats the steady-state lifetimes of carriers due to the presence of traps, to the case of sinusoidal carrier density fluctuations caused by sound waves. The effectiveness of traps is now modified

⁸ C. A. A. J. Greebe, Philips Res. Rept. **21**, 1 (1966).

⁹ C. A. A. J. Greebe, Phys. Letters **4**, 45 (1963).

¹⁰ E. Z. Meilikhov, Fiz. Tverd. Tela **7**, 1529 (1965) [English transl.: Soviet Phys.—Solid State **7**, 1228 (1965)].

¹¹ A. R. Moore and R. W. Smith, Phys. Rev. **138**, A1250 (1965).

¹² P. D. Southgate and H. N. Spector, J. Appl. Phys. **36**, 3728 (1965).

¹³ I. Uchida, T. Ishiguro, Y. Sasaki, and T. Suzuki, J. Phys. Soc. Japan **19**, 674 (1964).

¹⁴ C. A. A. J. Greebe, Solid State Commun. **3**, 227 (1965).

¹⁵ W. Shockley and W. T. Read, Phys. Rev. **87**, 835 (1952).

TABLE I. Values of physical constants for CdS.

	Shear coupling	Long. coupling	References
Sound velocity (10^5 cm/sec)	$v_S = 1.75$ 1.77 1.78	$v_L = 4.3$ 4.41 4.47	7 Computed from values in 16. Measured by us (in dark).
Elastic constant (10^{10} N/m ²)	$c_{44}^E = 1.487$ 1.505 ($\pm 0.2\%$)	$c_{33}^E = 9.37$ 9.38 ($\pm 0.2\%$)	a 16
Dielectric constant	$\epsilon_{11}^S/\epsilon_0 = 9.02$ ($\pm 0.5\%$)	$\epsilon_{33}^S/\epsilon_0 = 9.53$ ($\pm 0.5\%$)	16
Piezoelectric constant (C/m ²)	$e_{15} = -0.21$ -0.216 ($\pm 10\%$)	$e_{33} = +0.44$ +0.626 ($\pm 10\%$)	16 Computed from d 's in b and e 's in 16.
$\frac{1}{2}K^2$	0.018 0.0184 0.0194 ... 0.0177 0.0177	0.015-0.025 0.0121 0.0248 0.018 0.0387 0.0343	7 Computed from values in 16. Computed from d 's in b and other constants in 16. Empirical fit in 18. From $1 - K^2 = \epsilon^S/\epsilon^T$, using values in 16. K^2 from 16.
ω_D (300°K) (sec ⁻¹)	4.8×10^9 6.4	2.9×10^{10} 3.9	7 Computed from values in 16, using $\mu = 200$ cm ² /V sec.
Small-signal limit on strain	$S \ll 3.4 \times 10^{-5}$	$S \ll 4.2 \times 10^{-5}$	Computed from values in 16, using $\mu = 200$ cm ² /V sec.
Electron effective mass	$m^* = 0.2m_e$		c

^a H. J. McSkimmin, T. B. Bateman, and A. R. Hutson, J. Acoust. Soc. Am. 33, 856 (1961).

^b A. R. Hutson, Phys. Rev. Letters 4, 505 (1960).

^c W. S. Baer and R. N. Dexter, Phys. Rev. 135, A1388 (1964).

when the period of the acoustic wave becomes comparable to or less than the carrier lifetime and steady-state equilibrium cannot be reached. The generalization leads to a dependence of f on both frequency and conductivity. The approach assumes that only one impurity level is active in the trapping. The resulting expression for $\text{Re}(f)$ is^{8,9}

$$\text{Re}(f) = \left\{ \left[1 + \frac{n_1 N_T}{(n_0 + n_1)^2} \right] + \left[\frac{\omega}{\sigma_T v_{th} (n_0 + n_1)} \right]^2 \right\} / \left\{ \left[1 + \frac{n_1 N_T}{(n_0 + n_1)^2} \right]^2 + \left[\frac{\omega}{\sigma_T v_{th} (n_0 + n_1)} \right]^2 \right\}, \quad (12)$$

where n_0 is the equilibrium carrier density, N_T the trap density, σ_T the trapping cross section, v_{th} the electron thermal velocity, ω the acoustic frequency, $n_1 = N_e \times \exp(-E_T/kT)$ is the density of conduction electrons when the Fermi level lies at the trap, E_T the trap depth, and $N_e = 2(2\pi m^* kT/h^2)^{3/2}$.

The only conductivity dependence here is in n_0 , and although the functional form is complicated, we can see two limiting cases:

(i) High conductivity:

If $n_1 N_T / (n_0 + n_1)^2 \ll 1$, then

$$\text{Re}(f) = \frac{1 + [\omega / \sigma_T v_{th} (n_0 + n_1)]^2}{1 + [\omega / \sigma_T v_{th} (n_0 + n_1)]^2} = 1. \quad (13)$$

(ii) Low conductivity:

If $n_0 \ll n_1$, then

$$\text{Re}(f) = \frac{(1 + N_T/n_1) + (\omega / \sigma_T v_{th} n_1)^2}{(1 + N_T/n_1)^2 + (\omega / \sigma_T v_{th} n_1)^2} = \text{const} < 1. \quad (14)$$

In the intermediate region $\text{Re}(f)$ decreases monotonically with decreasing conductivity.

Whereas the shape of the acoustoelectric pulses is determined by the attenuation, their size is affected by trapping, and we shall find that amplitude measurements will yield information on trap depths and densities.

B. Magnitudes

Table I gives current values of the quantities that enter our expressions. Although only work on shear mode coupling will be reported here, the values for longitudinal coupling are included for completeness. We will use the values from Ref. 16 unless noted, as they represent the most recent and accurate measurements. Several comments can be made in the light of this table.

Our experimental work was done at an acoustic frequency of 30 MHz. Using the values of ω_D computed from Ref. 16, we find that

$$(\omega / \omega_D)_{\text{shear}} = 0.0294, \quad (\omega / \omega_D)_{\text{long}} = 0.0048.$$

¹⁶ D. Berlincourt, H. Jaffe, and L. R. Shiozawa, Phys. Rev. 129, 1009 (1963).

Thus we are perfectly justified in ignoring $(\omega/\omega_D)^2$ compared to 1, and to good approximation we can also neglect ω/ω_D compared to 1.

From the definition of f , we can see that we must have

$$|f| \leq 1,$$

and hence

$$|\operatorname{Re}(f)| \leq 1, \quad |\operatorname{Im}(f)| \leq 1. \quad (15)$$

Looking at Eq. (4), we see that we can drop the terms containing $\operatorname{Im}(f)$, and upon expanding the denominator we can also drop the $[\omega \operatorname{Re}(f)/\omega_D]^2$. We are thus left with

$$\alpha_E = \frac{1}{2} K^2 \frac{\sigma}{\epsilon v_s} \left[1 + \frac{2 \operatorname{Re}(f) \sigma}{\epsilon \omega_D} + \left(\frac{\sigma}{\epsilon \omega} \right)^2 \right]^{-1}. \quad (16)$$

When $\omega = 30$ MHz, the term containing $\operatorname{Re}(f)$ is small compared to the other two terms. In fact, changing $\operatorname{Re}(f)$ from 1 to 0 does not change the denominator by more than 3% at any conductivity, and by much less over most of the range. We choose to set $\operatorname{Re}(f) = 1$, giving the final expression for α_E :

$$\alpha_E = \frac{1}{2} K^2 \frac{\sigma}{\epsilon v_s} \left(1 + \frac{2\sigma}{\epsilon \omega_D} + \frac{\sigma^2}{\epsilon^2 \omega_D^2} \right)^{-1}. \quad (17)$$

It should be noted that, while α_E is insensitive to f , J_{AE} is proportional to $\operatorname{Re}(f)$, and hence it cannot be ignored there.

Equation (17) gives a bell-shaped dependence of α_E on $\ln \sigma$ (solid line in Fig. 7). Fortunately, the peak of the curve lies within our experimental range, so all facets of the function can be examined.

A wide range of values for the electromechanical coupling constant can be seen in Table I. This is due in part to the ϵ^2 dependence, which magnifies uncertainties in the values of ϵ .¹⁷ Some authors have chosen the value of $\frac{1}{2} K^2$ to fit the experimental data,¹⁸⁻²¹ and we are forced to take that path here. We feel that in the light of the wide spread of values this approach is justified.

We estimate that the largest possible effect of collision drag on the attenuation^{22,23} in the range of our measurements is 0.015 dB/cm; this is beyond our measurement limits.

C. Computational Extensions

The ideal exponential decay discussed above rarely occurs in practice. Some allowance for crystal inhomogeneity,

which badly distort acoustoelectric signals, must be made in order to permit any type of detailed analysis. Also, in order to get information on trapping it is advantageous to know the shape of the acoustoelectric current as sound is entering the crystal, as discussed below. Since the sound pulse shape can best be treated numerically, a computer program was written which follows the actual sound pulse envelope as it moves through the crystal and computes the macroscopic $I_{AE}(t)$ that should be observed in the experimental circuit. The crystal is treated as a large number of parallel slabs sliced perpendicular to the sound direction. Each slab is considered uniform over its volume, although different slabs may have different properties (e.g., f , μ , α , σ , W). The approximations involved in this model will be considered in detail below (Sec. 4).

A good example of an acoustoelectric pulse shape is shown in Fig. 2(d). The 30-MHz oscillations at the beginning and end of the traces are the first-order fields (E_1) due to the piezoelectric effect. They are visible only while sound is entering or leaving the crystal: Hence the region of interest for attenuation measurements is that between the oscillations, where the sound is entirely inside the crystal.

The point chosen as a measure of the size of the pulse, however, was its maximum value, even though at that point the sound is still entering. It is an easy value to measure accurately, and, although its location in time varies with different attenuations, this change in location is also automatically taken into account in the computer solution. There is a more important reason for choosing the peak height, however: It is fairly insensitive to α_L . In typical cases, changing α_L by 15 dB/cm (much more than observed values) changes $I_{AE(\text{peak})}$ by less than 20%. A point on the exponential tail, on the other hand, would be greatly influenced by α_L .

If we want to get an absolute value for $\operatorname{Re}(f)$ from I_{AE} , we must have absolute values for α_E , μ , and W . The attenuation can be measured from acoustoelectric shapes, as we shall see, to good accuracy. To get μ , Hall measurements were made on all crystals, and unless noted we have assumed $\mu = \mu_H$. (We will consider changes in μ due to trapping in Sec. 5.) But there is no way to get a good measure of W in this experiment, and we must be content with studying the relative dependence of $\operatorname{Re}(f)$ on conductivity. We can, however, get all the useful information from such a measurement.

When treating W , we will speak in terms of the maximum energy density at any point in the crystal at any time. When there is no amplification present, this will invariably occur at the input end of the crystal when the peak of the input sound pulse envelope enters; attenuation will reduce the sound amplitude at other points in the crystal. This maximum energy density is also independent of attenuation, and so

¹⁷ T. Ogawa and A. Kojima, Appl. Phys. Letters 8, 294 (1966).

¹⁸ A. I. Morozov, Fiz. Tverd. Tela 7, 324 (1965) [English transl.: Soviet Phys.—Solid State 7, 261 (1965)].

¹⁹ R. Truell, C. E. Elbaum, and A. Granato, J. Appl. Phys. 35, 1483 (1964).

²⁰ H. Kroger, Appl. Phys. Letters 4, 190 (1964).

²¹ A. I. Morozov, Fiz. Tverd. Tela 7, 3070 (1965) [English transl.: Soviet Phys.—Solid State 7, 2482 (1966)].

²² S. G. Eckstein, J. Appl. Phys. 35, 2702 (1964).

²³ H. N. Spector, J. Appl. Phys. 34, 3628 (1963).

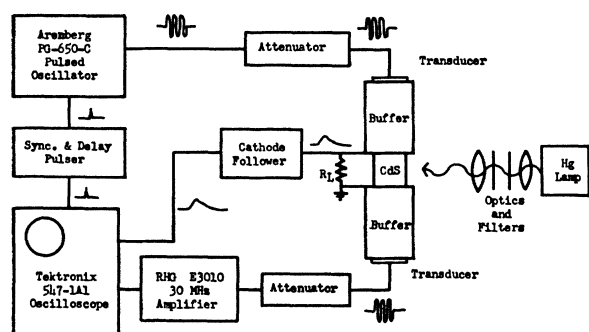


FIG. 1. Block diagram of the experimental system.

remains constant as the sample's conductivity is varied. It is also independent of any spatial inhomogeneities.

2. EXPERIMENTAL

Figure 1 shows the basic system used for examination of acoustoelectric waveforms. A pulsed oscillator and resonant quartz transducer (*Y* cut for shear mode operation) produce the 1- μ sec bursts of 30-MHz ultrasound that generate the acoustoelectric current pulses. This current develops a voltage across R_L which is displayed, via a cathode follower to eliminate distortion, on an oscilloscope. The sample is illuminated from op-

posite sides by a mercury lamp and appropriate spectral filters (the weakly absorbed 546- and 577-9- μ lines are used). The double illumination, together with careful alignment of the optical system, gave a light intensity uniform to better than $\pm 3\%$ over the entire crystal volume. This is necessary as nonuniform illumination has the same effect as nonuniform impurity distribution and would distort the acoustoelectric waveforms. Neutral density filters were used to control the sample's conductivity, although their calibration was not used and the sample's resistance was measured with an electrometer at each data point. Forced air cooling kept the sample at room temperature $\pm 1^\circ\text{C}$ under all operating conditions.

The CdS samples used were photoconductive and had high dark resistivity ($> 10^9 \Omega \text{ cm}$). Their orientation for shear operation had the *c* axis parallel to the end (acoustic bond) faces to within $\pm 0.5^\circ$. The ends were polished optically flat to eliminate mode conversion; nevertheless, extensive tests for mode conversion were carried out, the results showing that any unwanted modes were at least 35 dB below the main mode and hence unable to contribute any observable acoustoelectric signal.

Indium electrical contacts were applied to the ends of the crystals by a process of successive evaporation

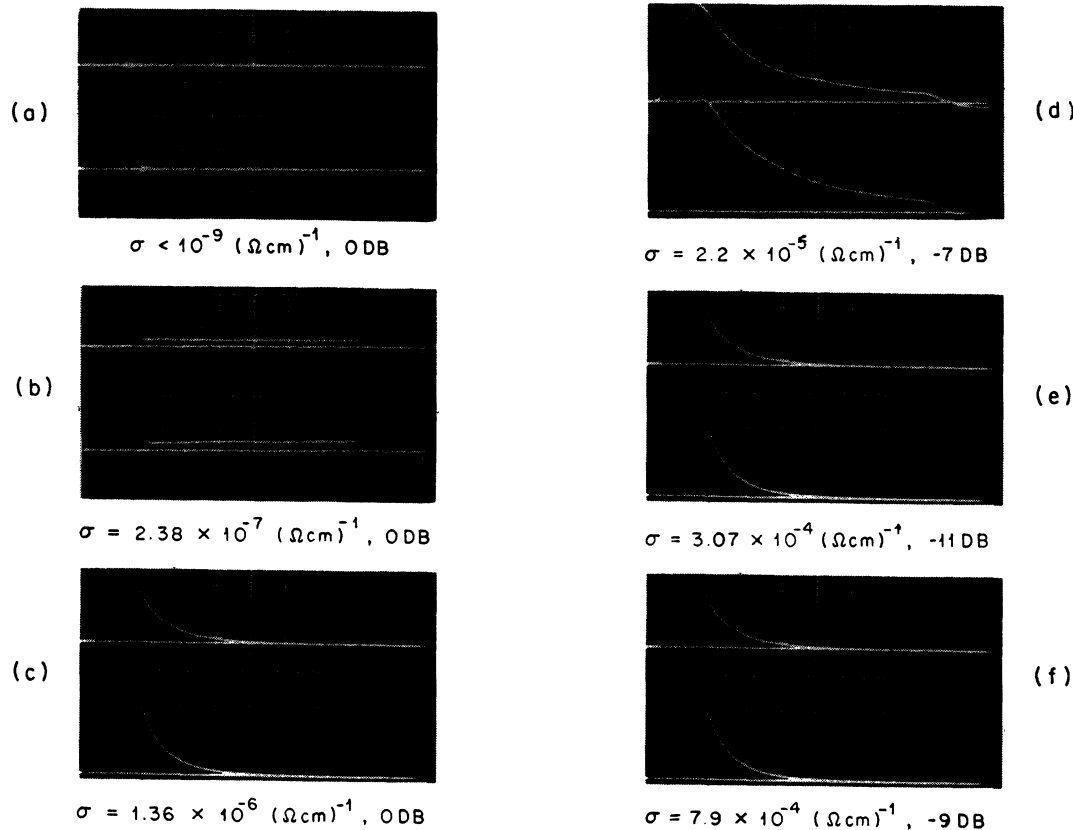
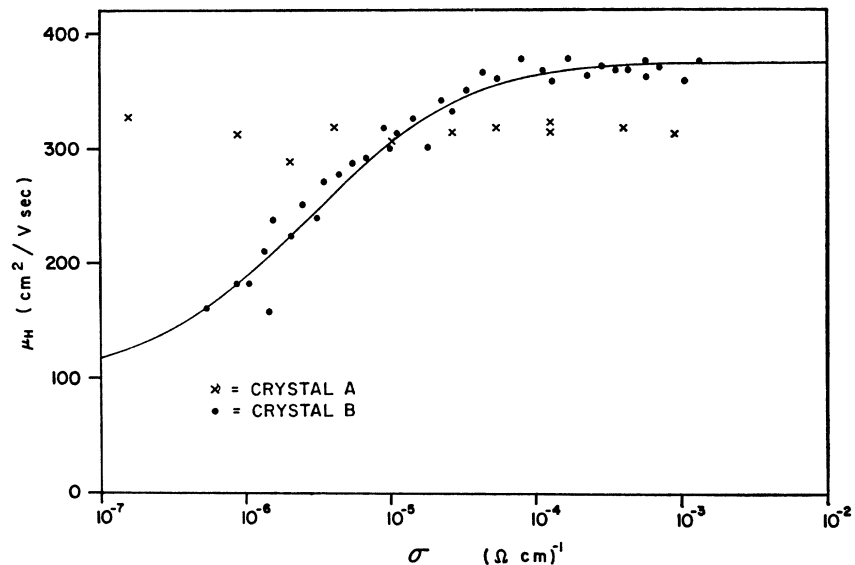
FIG. 2. Acoustoelectric waveforms for crystals A. Time base: 0.5 μ sec/cm. Vertical scale: 5 mV/cm.

FIG. 3. Measured Hall mobility versus conductivity.



and baking.²⁴ Since Ohmic contacts are notoriously difficult to obtain, extensive tests were made on each crystal after deposition of the electrodes. Potential probe, photovoltaic, and V - I linearity tests were performed in several ways, and no contacts were used if they showed any trace of non-Ohmicity.

3. RESULTS ON CRYSTAL A

Some of the acoustoelectric waveforms seen on what we shall call crystal *A* are shown in Fig. 2. The crystal is a 7-mm cube oriented for shear operation.²⁵ Its Hall mobility was measured as 315 $\text{cm}^2/\text{V sec}$, independent of conductivity (see Fig. 3). The two traces on each photo are for sound traveling in opposite directions through the sample assembly. Although the assembly is symmetric, it will be necessary to look at both directions in order to explain the observed pulse shapes. The two directions will be referred to as "sound in top" and "sound in bottom."

In the dark [Fig. 2(a)] α_E is so small that no signal is observable. Upon increasing the light intensity, α_E increases sufficiently to give a signal [Fig. 2(b)], but it is small enough that there is little loss of acoustic power, giving an almost constant I_{AE} . The bottom trace seems to rise slightly; this is not due to any amplification of sound, but occurs because the crystal is inhomogeneous (see Sec. 4). In Fig. 2(c) the attenuation of the sound wave can be seen, but the waveforms are not simple decaying exponentials. The irregularities are due to regions of differing conductivity. In Fig. 2(d) the traces look a great deal like the ideal case. (The input sound level has been reduced by 7 dB to keep the signals on scale.) The maximum α_E in this

crystal occurs in Fig. 2(e), where there is not enough acoustic power left to give any ac signal as it leaves the crystal. For high conductivity [Fig. 2(f)] α_E begins to decrease [right side of the peak in $\alpha_E(\sigma)$] with the output 30 MHz again visible. The acoustoelectric pulse shapes are quite different for the two directions, however, again due to nonuniform conductivity.

Since the sound-inside region of the acoustoelectric waveforms is not simply exponential, we must choose some method of analyzing the data that will retain as much information as possible. We choose to *force* a simple exponential least-squares fit to the data, thus averaging over some of the inhomogeneity. It will still be possible, however, to see the effects of gross conductivity gradients, and all of the essential features of the waveforms are retained. The experimental points to be fitted are read off photographs similar to Fig. 2, but using expanded scales for greatest accuracy.

Data on crystal *A* from several runs are plotted in Fig. 4. The solid and open circles represent sound traveling in opposite directions. The two pulses in Fig. 2(f) appear here as different attenuations for sound traveling in different directions. Of course, for a sound wave traveling the entire length of the crystal, the total attenuation must be the same for either direction; so we will call the ordinate "apparent attenuation." The solid line is the total attenuation, using $\frac{1}{2}K^2 = 0.0142$ in Eq. (17) for α_E , and $\alpha_L = 0$, both chosen for best fit. K^2 determines the size of the curve, while α_L merely shifts it up or down. As these are the only variables at our disposal, there is no way of accounting for the difference in conductivity of the peaks of the theoretical and experimental curves. A possible explanation for this will be presented in the next section.

Several comments can be made in the light of Fig. 4. Even though theory and experiment do not quite co-

²⁴ V. E. Henrich, thesis, Department of Physics, University of Michigan, 1967 (unpublished).

²⁵ This crystal was given to us by Dr. B. Tell.

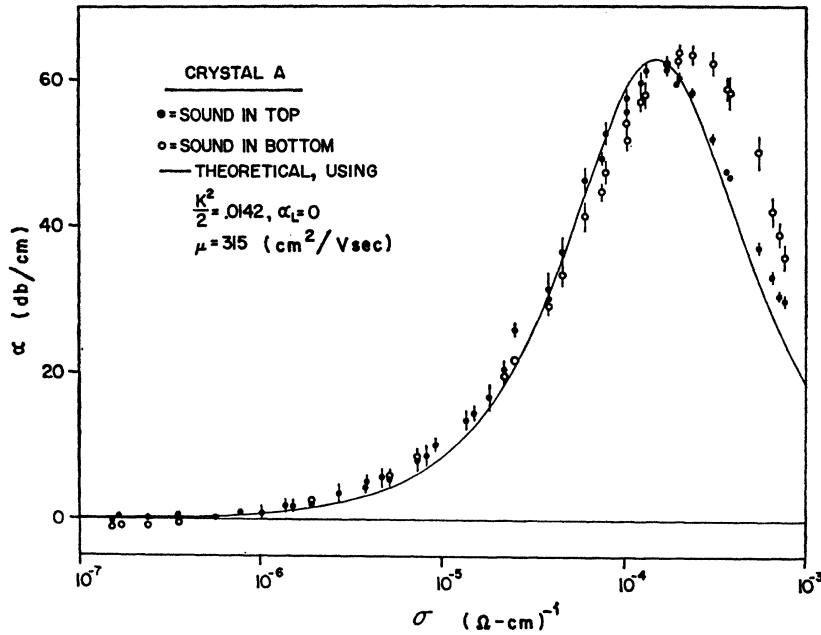


FIG. 4. Attenuation versus conductivity for crystal A.

incide, particularly near the peaks, the general agreement is fairly good. There is not much leeway in the choice of α_L ; only $\alpha_L < 2 \text{ dB/cm}$ will allow any sort of decent fit to the majority of the points, and this fit is reasonably independent of behavior around the peak. The value of $\frac{1}{2}K^2$ is only about 20% below the computed values in Table I.

The "shape" measurement above has given the ultrasonic attenuation; we shall next consider the "size" measurement. For runs involving absolute size of acoustoelectric pulses, the input sound level was held constant (0 dB) and the oscilloscope's vertical sensitivity changed to accommodate the pulses. Since bond effici-

encies do enter in this type of measurement, runs taken with different assemblies, or even on different days with the same assembly, cannot be compared. All results quoted for these measurements are for a single run, taken as rapidly as possible, and after precautions had been taken to assure that the crystal and buffers would remain at constant temperature during the run. Figure 5 shows the results of such a run on crystal A. Corrections for the finite size of the load resistor R_L have been made, and the ordinate is the short-circuit value of I_{AE} . It is not surprising that there are two distinct curves for sound going in opposite directions here, since each direction corresponds to a different

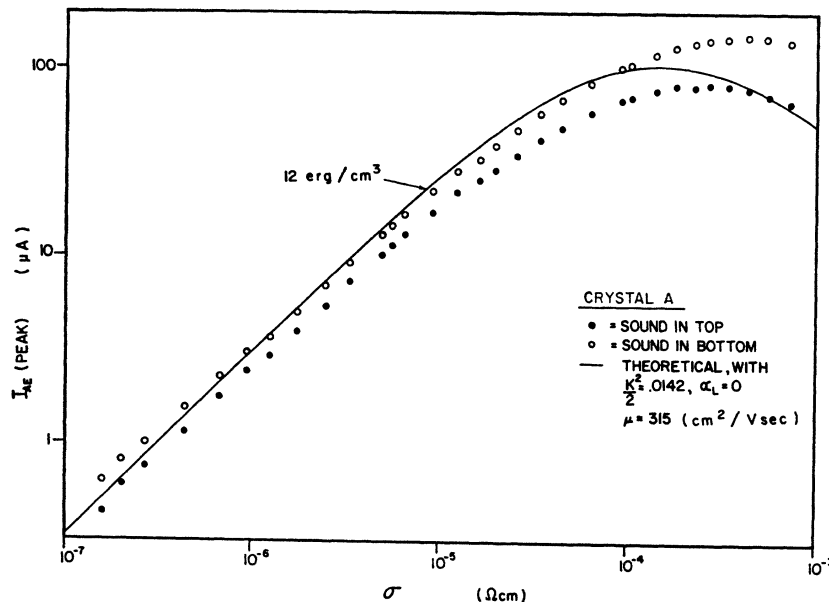


FIG. 5. Peak acoustoelectric current versus conductivity for crystal A.

input transducer, buffer, and bonds. The closeness of the curves indicates that the bonds are very nearly the same throughout the system. The peak current has been plotted on a logarithmic scale since the quantities that we are not sure of [i.e., W , possibly $\text{Re}(f)$ and μ] enter multiplicatively [see Eq. (6)]. Thus a change in acoustic power level corresponds to sliding the curves up or down. The solid curve is the computer-predicted $I_{\text{AE}(\text{peak})}(\sigma)$ for a maximum energy density of 12 erg/cm³, assuming $\text{Re}(f)=1$, $\mu=315$ cm²/V sec, and $\frac{1}{2}K^2=0.0142$. This power level was chosen to roughly fit both curves; attempts to accurately fit either curve would not be significantly more successful. For one thing, we see here, as in Fig. 4, that the experimental data peak at higher conductivity than the theory, and also that "sound in bottom" peaks at slightly higher conductivity than does "sound in top."

One might ask whether allowing $\text{Re}(f)$ to vary with conductivity might give a better fit to the data. We saw above [Eq. (12)] that $\text{Re}(f)$ will either be constant or will decrease with decreasing conductivity. To get a better fit on the low conductivity side of Fig. 5 we would have to increase $\text{Re}(f)$ slightly with decreasing conductivity, however. The fact that the fit to experiment is as good as it is from 10^{-7} to 10^{-4} (Ω cm)⁻¹ leads to the conclusion that $\text{Re}(f)$ is nearly constant, and hence presumably equal to 1. So trapping does not seem to be important in this crystal.

4. CRYSTAL INHOMOGENEITY

The measurements on crystal *A* indicate that the ultrasonic attenuation is not constant throughout the crystal at a given light intensity. We attribute this to a nonuniform spatial distribution of impurities, since CdS is an impurity photoconductor for wavelengths longer than 520 m μ , and since electron diffusion lengths are short enough that the conductivity will reflect the impurity distribution. The purpose of this experiment is to study attenuation, trapping, etc., in CdS, not to map out in detail the impurity distribution in particular crystals. Yet some efforts must be made in this direction if we are to make any progress in understanding the results obtained on real crystals.

All of our crystals were grown by a vapor-phase technique.^{26,27} By nature of the growth process, we have no *a priori* reason to expect any particular spatial impurity distribution. The location of the crystals in the original boules is not known, and even that would give only slight hints. In general, the inhomogeneity can be described in terms of variations in three spatial directions: two perpendicular to the sound velocity (transverse) and one parallel to it (longitudinal). If the variation were purely transverse, it would not give rise to different acoustoelectric waveforms for sound

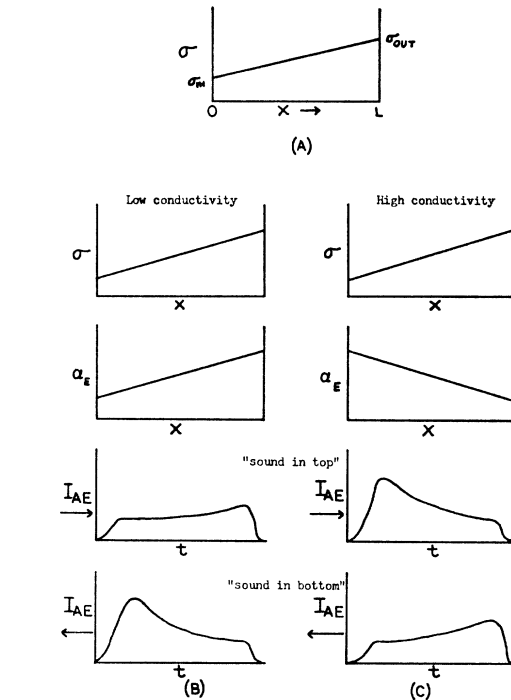


FIG. 6. Crystal conductivity gradient and associated acoustoelectric pulses.

traveling in opposite directions. A longitudinal variation, however, would give different pulse shapes. The mathematical treatment of this last case is relatively easy, since we still have straight-line current flow.

A. Longitudinal Impurity Gradient

We will consider only the simplest possible model: a linear change in impurity density from one end of the crystal to the other. While we would expect quantitative agreement to be poor, the qualitative results will tell us whether or not we are on the right track. Since the electrical conductivity should be proportional to impurity density, we will talk in terms of a linear change in conductivity [see Fig. 6(a)]. Two parameters are necessary to completely specify this distribution. The only one macroscopically available is R_c , the bulk crystal resistance. From this we can define an "observed conductivity" σ_0 :

$$\sigma_0 = L/AR_c, \quad (18)$$

where L is the length of the crystal and A its area. The other parameter we will use is

$$\gamma \equiv \sigma_{\text{out}}/\sigma_{\text{in}}. \quad (19)$$

This will be chosen to give a best fit to the data. Assuming that σ is a linear function of position x , we can express it in terms of these two parameters:

$$\sigma(x) = \frac{\sigma_0 \ln(\gamma)}{\gamma - 1} \left[1 + (\gamma - 1) \frac{x}{L} \right]. \quad (20)$$

²⁶ L. Clark and J. Woods, Brit. J. Appl. Phys. **17**, 319 (1966).

²⁷ E. D. A. White, Brit. J. Appl. Phys. **16**, 1415 (1965).

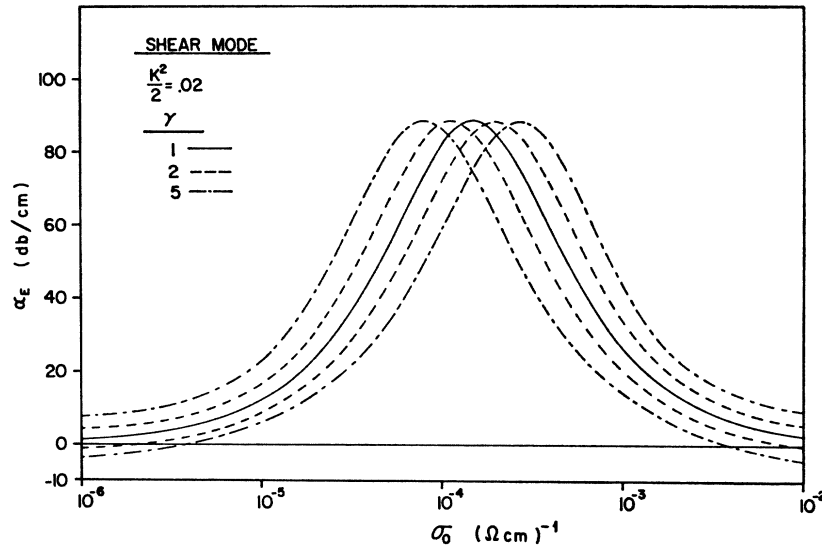


FIG. 7. Predicted apparent attenuation versus observed conductivity for longitudinally nonuniform crystal.

In keeping with the simplicity of the model, we will assume that γ is a constant for a particular crystal independent of conductivity. The validity of this assumption is, unfortunately, a complicated function of the trapping kinetics, and for a crystal with as large and diffuse an impurity content as CdS we could never hope to predict a dependence which we could be sure was any better than the above one.

It is instructive to look at the pulse shapes predicted by the above model for two limiting cases. First, consider the case of low conductivity in which α_E is small and also increases as σ increases [Fig. 6(b)]. Suppose that α_E is small enough that in a homogeneous crystal the acoustoelectric signal would be nearly flat. As the sound pulse moves down the crystal, it enters regions of higher and higher α_E , and hence larger and larger I_{AE} . We would then see an acoustoelectric signal which actually rises. This is just the case seen in Fig. 2(b) in crystal *A*. Sound traveling in the other direction enters in a region of large α_E , and hence large I_{AE} , and moves into regions of smaller α_E . We would then see a signal which decays more rapidly than for a homogeneous crystal. In the general case of α_E large enough to produce a decaying signal in a homogeneous crystal, the distinct rise in the first case would not be seen, but the decay would be more gradual (less apparent attenuation) than normal; sound going in the other direction would give a steeper decay (more apparent attenuation) than normal. In the case of high conductivity α_E will decrease as σ increases [Fig. 6(c)], and the roles of the two sound directions will be interchanged; the limiting case of small α_E is shown in the figure.

The $I_{AE}(t)$ waveforms computed using the above conductivity model will not be exactly exponential. Since we treat the experimental data by forcing an exponential fit to them, we choose to do the same with the predicted pulse shapes. The computer first gener-

ates the entire pulse and then fits only the "sound inside" part. It gives both the apparent attenuation and its standard deviation. In all cases that we will consider the standard deviations are too small to be included on the graphs, indicating that the pulses are nearly exponential. The strength of this method lies in the fact that both theory and experiment are treated in exactly the same manner. The graphs now display "apparent attenuation" versus "observed conductivity", but there is a one-to-one correspondence between theory and experiment.

Figure 7 shows the predicted $\alpha(\sigma)$ for γ 's of 1 (homogeneous crystal), 2 and 5 for typical parameters. As γ increases, the curve splits into two branches, one for sound in each direction; the splitting increases with increasing γ . The negative values correspond to acoustoelectric pulses that rise, as in Fig. 6, and not to actual gain. In agreement with the predictions of Fig. 6, the roles of sound in opposite directions are interchanged between high and low conductivity. For values of γ as large as 10, a nonzero α_L merely shifts the curves up, as in the homogeneous case. Several trials with large γ 's and large α_L 's showed that the error incurred in just shifting the curves by α_L is negligible in all cases of interest.

As a direct check on the results of a longitudinal conductivity variation, the light incident on a sample was purposely made nonuniform. Sound was always sent in the same direction so that crystal irregularities would not enter. One-half of the crystal was masked with a strip of 0.3 neutral density filter (50% transmission) and photos of the acoustoelectric pulses when the filter was masking different ends of the sample were taken. Here the masking of different ends corresponded to sound going in opposite directions in our usual measurements. The results were as predicted above, with the masking that gave higher apparent attenuation at low conductivity giving lower attenua-

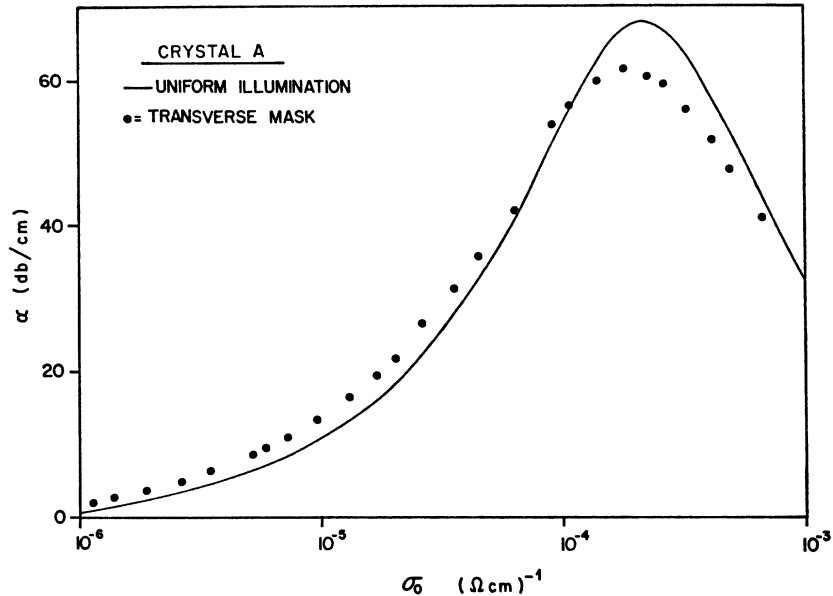


FIG. 8. Apparent attenuation versus observed conductivity for transversely masked crystal.

tion at high conductivity, and vice versa. The size of the apparent attenuations was also in general agreement with theory, although extensive measurements were not made.

A qualitative comparison of Fig. 7 with Fig. 4 for crystal *A* shows that while we may be moving in the right direction we are not there yet. The experimental curves are only split at high conductivity, while the theoretical ones show the same splitting at all points. It might be possible to construct a fit by taking $\gamma=1$ at low conductivities and increasing to something near 2 at the high end. But this would be doctoring with no particular justification. Yet one should bear in mind that keeping γ constant is merely an assumption, and it is quite possibly not a good one for this crystal. Another point of disagreement is that the two experimental curves are not symmetric about the theory, and we would have to do some horizontal translation to make them so. Also, the rightmost curve has a larger maximum than does the other, something not predicted by our model. These considerations show that the simple model used here is not sufficient to fully explain the attenuation data on crystal *A*, although it does at least predict a splitting of the curve.

Curves for the predicted $I_{AE(\text{peak})}(\sigma)$ for various values of γ were also computed. These curves obey the same general rules as $\alpha(\sigma)$, with the splitting nearly symmetric about the uniform case. Minor irregularities occur at high and low conductivities corresponding to regions in which one acoustoelectric pulse rises; the position of $I_{AE(\text{peak})}$ then shifts to the output end of the crystal. Behavior similar to that has been observed. The curves for sound in either direction can still be raised or lowered individually, depending on the acoustic power received from either end. Comparison with

the data for crystal *A* showed the same qualitative similarities and disagreements as for $\alpha(\sigma)$.

B. Transverse Impurity Gradient

Any purely longitudinal conductivity variation, no matter how large or irregular, still gives straight-line acoustoelectric current flow, and the problem can be rigorously and easily solved. A transverse gradient, on the other hand, leads to a problem of immeasurably greater difficulty. Different sections of a sound wave will be attenuated different amounts in traveling the same distance down the crystal, due to the different conductivities of the paths, giving rise to complicated current patterns. We have not undertaken a mathematical solution of this problem, but one can get some idea of what to expect by considering extreme cases.

Suppose that the crystal were composed of two parallel sections, one a semiconductor and the other a perfect insulator, whose interface was parallel to the sound velocity. The sound wave would generate an acoustoelectric signal only in the semiconducting section, and the $I_{AE}(t)$ would have the same shape as if the whole crystal were semiconducting. Our measurement of R_c , however, would yield a value of σ_0 smaller than the actual σ . In other words, the experimental data would be displaced toward lower conductivity. Similarly, if part of the crystal were always more highly conducting than the semiconducting part, we would plot the data at higher conductivity than it belonged. Both $\alpha(\sigma)$ and $I_{AE(\text{peak})}(\sigma)$ data would be displaced by the same amount.

The problem of a transverse gradient can be simulated experimentally. The light incident on crystal *A* was made transversely nonuniform by masking one-

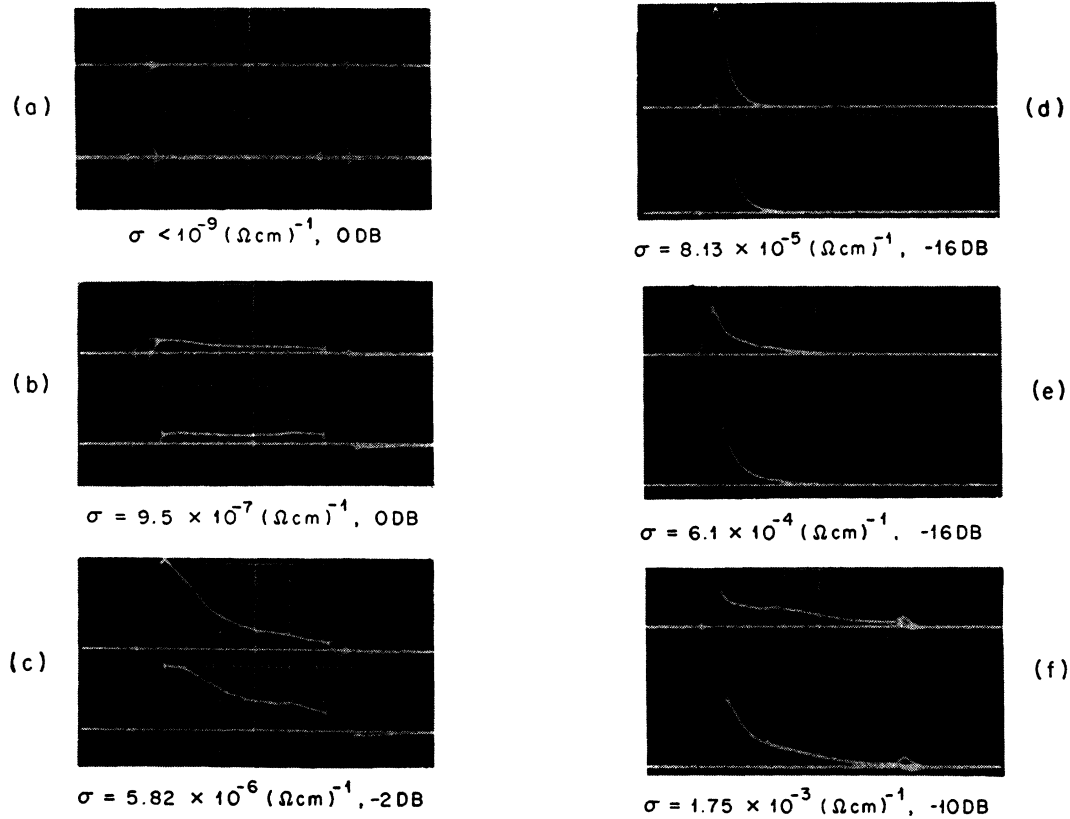


FIG. 9. Acoustoelectric waveforms for crystal *B*. Time base: 1 $\mu\text{sec}/\text{cm}$. Vertical scale: 5 mV/cm.

half of it lengthwise with pieces of 0.8 neutral density filter (16% transmission). In Fig. 8 the solid curve is a measurement of $\alpha(\sigma)$ by acoustoelectric pulse shapes when the crystal is uniformly illuminated and the dots are the same measurement with the neutral density masks. Not only can the shift of the curve toward lower conductivity be seen, but a substantial flattening of the curve as well. The analogous case of high conductivity in one section could not be simulated with our light source.

Any crystal that has a longitudinal component of conductivity gradient probably also has transverse components of the same magnitude. We believe that such gradients are the cause of some or all of the displacements of the data seen in our crystals, as well as playing a part in other deviations of the data from theory.

5. RESULTS ON CRYSTAL *B*

Rather than trying to fit the data on crystal *A* any further by the above considerations, we shall look at a second crystal. To be called crystal *B*, it is a 1-cm cube also oriented for shear operation. Its measured Hall mobility is somewhat conductivity-dependent. Its acoustoelectric waveforms behave as expected, and its attenuation fits the conductivity gradient model

very closely. In addition, it shows strong evidence of trapping.

A. Hall Mobility

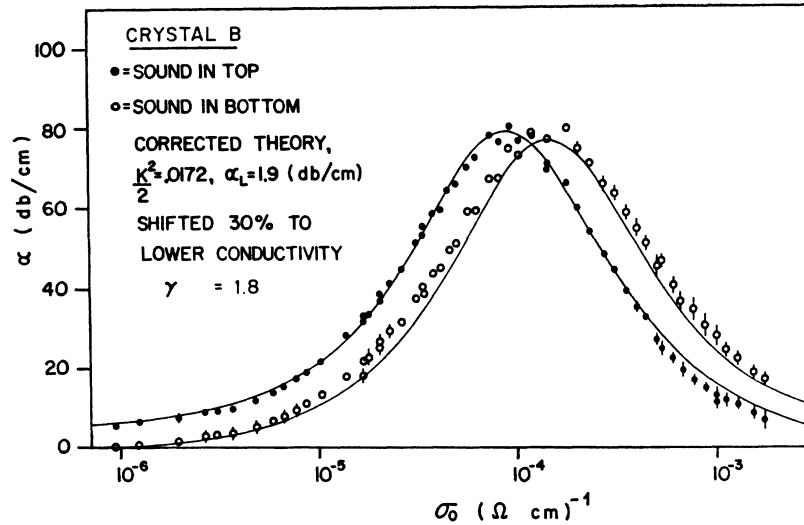
Figure 3 gives the measured variation of μ_H with σ for crystal *B*, where the solid line is the theory which we shall apply. Bube and MacDonald²⁸ have observed similar changes in μ_H in CdS and were able to explain them in terms of the changing charge state of scattering centers. Consider a donor level lying above the dark Fermi level. It will be ionized at low light intensities and will have a large scattering cross section. As the electron Fermi level rises with increasing light intensity, the level will become occupied and thus have a smaller cross section. The expression derived for this process is²⁸

$$\frac{1}{\mu_H} = \frac{1}{\mu_\infty} + \frac{\beta v_{th} S_+ N_+}{1 + 2 \exp[(E_+ - E_{fn})/kT]}, \quad (21)$$

where μ_∞ is the Hall mobility with all donors occupied (bright light), v_{th} is the electron thermal velocity, $\beta = 5.7 \times 10^{-16}$ V sec²/cm², S_+ is the donor scattering cross section when ionized, N_+ the density of donors,

²⁸ R. H. Bube and H. E. MacDonald, Phys. Rev. **121**, 473 (1961).

FIG. 10. Attenuation versus conductivity for crystal B.



E_+ the depth of donor below conduction band, and E_{fn} the electron Fermi level. Since this gives $1/\mu_H$ as a function of E_{fn} , conductivities were converted to Fermi levels by

$$\sigma/e\mu = n = N_c \exp(-E_{fn}/kT), \quad (22)$$

where $N_c = 2(2\pi m^* kT/h^2)^{3/2}$.

The mobility data were fit to the above expression by least squares, yielding values of

$$\begin{aligned} \mu_{\infty} &= 374 \text{ cm}^2/\text{V sec}, \\ \beta v_{th} S_+ N_+ &= 7.55 \times 10^{-3} \text{ V sec/cm}^2, \\ E_+ &= 0.447 \text{ eV}. \end{aligned}$$

The solid line in Fig. 3 is Eq. (21) using the above numbers, and the fit is excellent. The magnitude of the parameters is also reasonable. The trap depth agrees with a prominent group of levels at 0.40–0.45 eV reported by several authors.^{8,10,29} The value of S_+ observed in CdS in Ref. 28 is about 10^{-10} cm^2 , and using that value gives $N_+ = 6.3 \times 10^{15} \text{ cm}^{-3}$.³⁰ So the Hall mobility variations in crystal B seem to be due predominantly to the changing charge state of deep traps, with good quantitative agreement with theory.

B. Acoustoelectric Measurements

Figure 9 shows representative acoustoelectric pulse shapes for crystal B. Only a few comments are necessary about them. With low light intensity, Figs. 9(b) and 9(c), the effect predicted earlier is clearly seen; “sound in top” has a larger apparent attenuation than “sound in bottom,” characteristic of a longitudinal conductivity gradient. Near the maximum in $\alpha_B(\sigma)$ [Fig. 9(d)] both directions look the same, and in brighter light [Figs. 9(e) and 9(f)] the roles of the directions are

interchanged, with “sound in bottom” now having larger attenuation. The unevenness of Figs. 9(b), 9(c), and 9(f) shows that the impurities do not vary smoothly down the crystal.

Figure 10 gives the least-squares-fit attenuation for this crystal, taken on three runs. The theoretical curves included are based on an analysis of $I_{AE(\text{peak})}$ data as well as the attenuation and will be discussed shortly.

Data on $I_{AE(\text{peak})}(\sigma)$ are plotted in Fig. 11. The solid curves are theoretical for $\gamma = 1.8$, $\frac{1}{2}K^2 = 0.0172$, and $\mu \text{Re}(f) = 374 \text{ cm}^2/\text{V sec}$ and constant. This value of γ was determined as a result of fitting all the data on this crystal and is not obvious at this stage in the analysis. The theoretical curves have been fit to the data at high conductivity because of the variation of μ —having its largest, constant value at large σ —and because of the predicted dependence of $\text{Re}(f)$. There is good agreement over one order of magnitude at large σ , but the disagreement is as great as a factor of 20 at $10^{-6} (\Omega \text{ cm})^{-1}$. We must thus explain the large discrepancy between theory and experiment and see what effect it will have on attenuation measurements.

C. Trapping

We saw above that α_B is only weakly dependent on μ and $\text{Re}(f)$. [Note that μ appears in the denominator of the term containing $\text{Re}(f)$ in Eq. (16), since $1/\omega_D = D_n/v_s^2 = \mu kT/qv_s^2$.] The computer should then predict the correct W for all points and times even if there are large changes in μ or $\text{Re}(f)$. Any deviations of experiment from what is predicted must then come from $\mu \text{Re}(f)$ in Eq. (6). Since μ_H only varies by a factor of 2 over the 10^{-6} – $10^{-2} (\Omega \text{ cm})^{-1}$ range, the remaining discrepancy must be due to a conductivity variation of $\text{Re}(f)$.

The method of determining $\text{Re}(f)$ from $I_{AE(\text{peak})}(\sigma)$ data is somewhat involved and tiresome, and we shall only outline it here. Full details can be found in Ref.

²⁹ U. Büget and G. T. Wright, Brit. J. Appl. Phys. 16, 1457 (1965).

³⁰ The authors are grateful to Dr. J. D. Zook for calling their attention to the correct cross section.

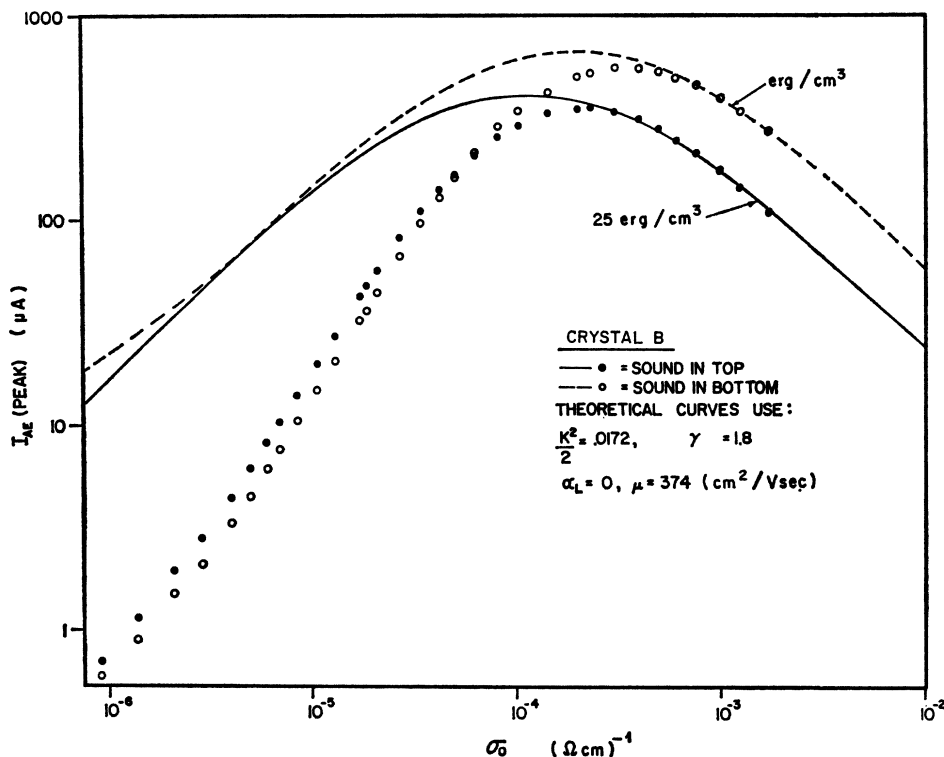


FIG. 11. Peak acoustoelectric current versus conductivity for crystal B.

24. First, a value of γ is assumed and theoretical $I_{AE(peak)}(\sigma)$ curves are computed. Then the ratio of experimental to theoretical values is taken, and since the theory assumes $Re(f)=1$ and $\mu=\mu_\infty$, we get

$$\frac{I_{AE(peak)}(\text{experimental})}{I_{AE(peak)}(\text{theoretical})} = (\mu/\mu_\infty) Re(f).$$

When this is done for both directions of sound, two

curves are obtained, similar in shape but separated in conductivity. This is because $I_{AE(peak)}$ occurs just as the sound is entering the crystal, and so the different directions see different conductivity regions. To correct for this, the two curves derived above are shifted in conductivity until they coincide, and the ratio of conductivities at positions of peak current necessary for such a shift is computed. This ratio should be 10-20% less than γ since the sound is partly inside, and values

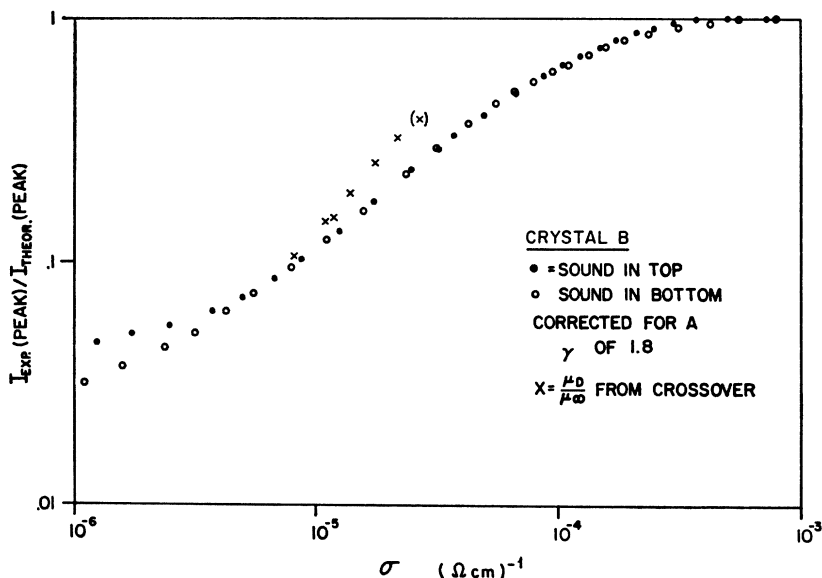


FIG. 12. Ratio of experimental to theoretical peak acoustoelectric current versus conductivity for crystal B, corrected for crystal inhomogeneity.

of γ are tried until the two ratios are consistent. This method is very sensitive to γ , and for these data values of 1.6 and 2.0 gave unreasonable results, while $\gamma=1.8$ gave consistent results. The results of this procedure are plotted in Fig. 12. The curves coincide over most of the experimental range, disagreeing only for low conductivities where, due to rising waveforms, $I_{AE(\text{peak})}$ can occur at either end of the crystal.

There is an independent method of checking these data. If a dc electric field is applied to the sample as for ultrasonic amplification, the field necessary to restore an acoustic pulse to its amplitude in the dark is given by¹²

$$E_{dc} = v_s / \mu \text{Re}(f),$$

where v_s is the velocity of sound. There are many problems with such measurements,^{2,31} and they could only be performed over a small range of conductivity on this crystal. The results, divided by $\mu_\infty = 374 \text{ cm}^2/\text{V sec}$, are plotted as X 's in Fig. 12. The agreement is fairly good, with the disagreement possibly due to the high electric fields used somewhat reducing trapping,³² bringing $\text{Re}(f)$ closer to 1.

Knowing $\mu(\sigma)$ from Hall measurements, μ may be divided out of the data in Fig. 12, yielding $\text{Re}(f)$ alone. The resulting curve can then be fit to the expression given in Sec. 1. The trapping cross sections seen for traps in the 0.4–0.45-eV range are in the neighborhood of 10^{-14} cm^2 .⁸ Using this for σ_T , the only unknowns in Eq. (12) are E_T and N_T . By adjusting these parameters, a good (and unique) fit could be obtained to the data. The parameters derived were $E_T = 0.39 \text{ eV}$ and $N_T = 3.6 \times 10^{15} \text{ cm}^{-3}$. The value of E_T is close to the 0.4–0.45-eV levels, and the trap density agrees well with values determined from measurements as a function of frequency.⁸ Both values also agree fairly well with those determined by fitting the Hall mobility data. So the effects of trapping observed in this crystal can be well explained by Greebe's theory, yielding values in good agreement with other observations.

We must now consider what effect a variation in $\mu \text{Re}(f)$ will have on attenuation measurements. We have seen that α_E and W are nearly unaffected by $\mu \text{Re}(f)$, but since we use the acoustoelectric pulse

shapes to determine attenuation, there may be complications. If the crystal were homogeneous, changes in $\mu \text{Re}(f)$ with conductivity would affect the size of $I_{AE}(t)$ but not its shape. But if the crystal is nonuniform, $\mu \text{Re}(f)$ will vary with position and give the same behavior as a changing α_E . Both $\mu(\sigma)$ and $\text{Re}(f)(\sigma)$ were put into the computer program, and correct values of $\alpha_E(\sigma)$ were obtained. The curves agree well with the data except that they peak at somewhat higher conductivity (about 30%) than the data. This is in the opposite direction to the effect seen in crystal *A*, and since it may be due, at least in part, to transverse conductivity gradients, we will take the liberty of moving the theoretical curves slightly toward lower conductivity. [We will not bother to shift the theoretical values of $I_{AE(\text{peak})}(\sigma)$. Such a shift would make some changes in $\text{Re}(f)(\sigma)$, leading to slightly smaller values. But such changes would make virtually no difference in the attenuation predictions, and the new $\text{Re}(f)(\sigma)$ would yield very nearly the same trap depth and concentration.]

The solid curves in Fig. 10 give the corrected, "shifted" theory. Considering the simplicity of our model of impurity distribution, the agreement is very good. The assumption of constant γ over the whole conductivity range is apparently valid for this crystal. The value of $\alpha_L = 1.9 \text{ dB/cm}$ is determined by the asymptotic fit at low and high conductivities. The value of $\frac{1}{2}K^2$ is also very close to those calculated in Table I. The value may actually be a bit higher than 0.0172, since we saw in Fig. 8 that a transverse gradient reduced the size of $\alpha(\sigma)$ as well as shifting it, but we have no quantitative way of treating this.

In summary, all aspects of this crystal can be readily explained in terms of fairly elementary considerations. Its Hall mobility is well described by the changing charge state of a deep impurity level. Electron trapping is observed and can be accounted for by a deep trap whose level and density agree well with measurements made by other methods. The attenuation data show excellent agreement with the theory of Hutson and White, taking into account impurity inhomogeneity.

ACKNOWLEDGMENT

The authors would like to thank J. H. Gibson for assistance with the computer calculations and for many helpful discussions.

³¹ A. R. Hutson, J. H. McFee, and D. L. White, Phys. Rev. Letters **7**, 237 (1961).

³² D. L. White (private communication).

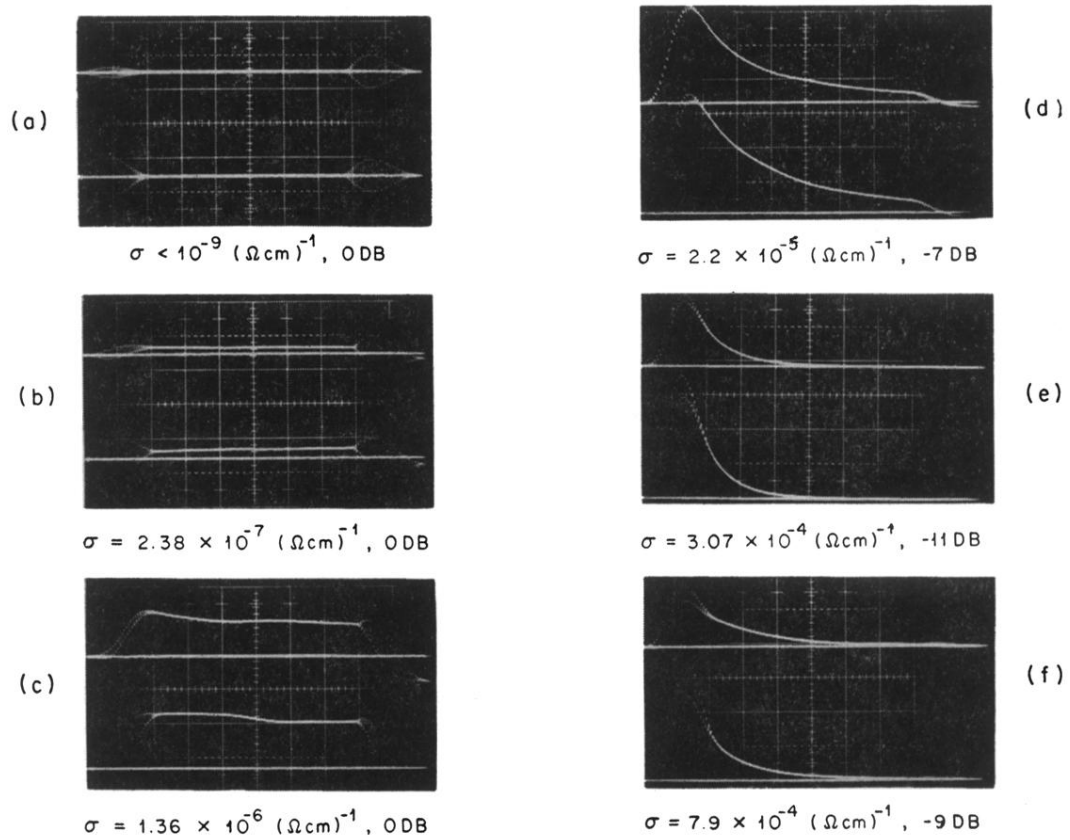


FIG. 2. Acoustoelectric waveforms for crystals *A*. Time base: 0.5 $\mu\text{sec}/\text{cm}$. Vertical scale: 5 mV/cm.

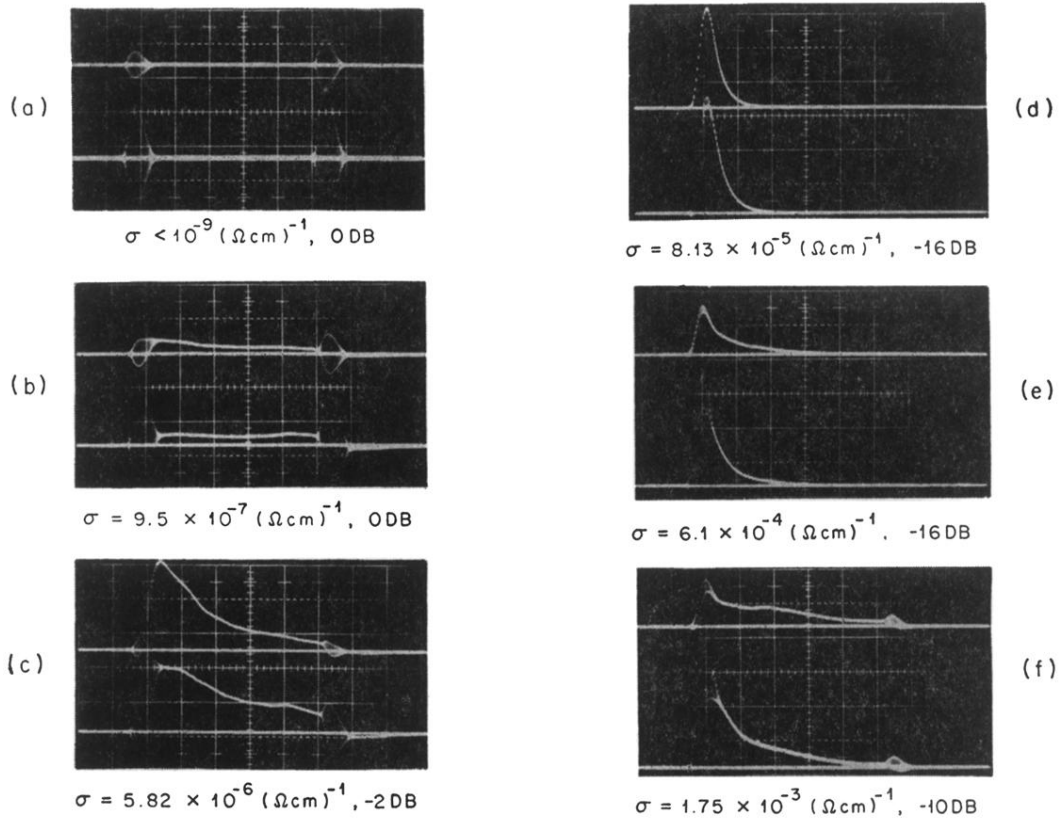


FIG. 9. Acoustoelectric waveforms for crystal *B*. Time base: 1 $\mu\text{sec}/\text{cm}$. Vertical scale: 5 mV/cm.